Cement and Concrete Research 42 (2012) 945–952

Contents lists available at SciVerse ScienceDirect

Cement and Concrete Research

journal homepage: http://ees.elsevier.com/CEMCON/default.asp

Water permeability of reinforced concrete with and without fiber subjected to static and constant tensile loading

C. Desmettre, J.-P. Charron *

Research Center on Concrete Infrastructure (CRIB), École Polytechnique de Montréal, Montréal, Canada

ARTICLE INFO

Article history:
Received 25 October 2011
Accepted 20 March 2012

Keywords:
Concrete (E)
Fiber reinforcement (E)
Permeability (B)
Tensile properties (B)
Self-healing

ABSTRACT

In this study, an innovative permeability device allowing permeability measurement simultaneously to loading was used to investigate the water permeability and self-healing of reinforced concrete. The experimental conditions focused on normal strength concrete (NSC) and fiber reinforced concrete (FRC) tie specimens under static and constant tensile loadings. Crack pattern and crack openings under the same loadings were measured on companion specimens. Experimental results emphasized the positive contribution of fibers to the durability of reinforced concrete. Under static tensile loading, the FRC tie specimens were 60% to 70% less permeable than the NSC tie specimens at the same level of stress in the reinforcement. After 6 days of constant loading, the FRC showed greater self-healing capacity with a reduction in water penetration of 70% in comparison to 50% for the NSC. The main cause of self-healing was the formation of calcium carbonate ($CaCO_3$).

1. Introduction

A large proportion of reinforced concrete structures present durability problems (steel corrosion, chemical attacks by chlorides and sulfates, freeze–thaw damage, carbonation, etc.) before reaching their design life. Most of these deteriorations are due to ingress of water and aggressive agents into the concrete. Three transport modes can occur in structures: diffusion (due to a concentration gradient), permeability (due to a pressure gradient) and capillarity suction (due to capillarity effects). Transport by diffusion occurs typically in structures exposed to severe environment (chloride, sulfate ions, etc.) for which the ions concentration is higher outside than inside the concrete. Transport by permeability is predominant for structures submitted to high pressure (dams, liquid containments, nuclear power plant containments, etc.), but may also occur under smaller pressure gradients in other exposed structural elements (beams, slabs, walls, etc.). Transport by capillarity suction occurs for example when a structure is subjected to wet–dry cycles. Depending on the kind of structures, the three transport modes can occur simultaneously. Nevertheless, one of these modes is often predominant.

Numerous parameters can modify the transport properties in reinforced concrete structures (concrete type, concrete cover, rebar type, reinforcement ratio, presence of cracks (resulting from environmental or mechanical loadings) and their healing capacity). Reinforced concrete structures are usually cracked in service. Cracks create favorable paths for fluids penetration; which can significantly modify the transport properties into the structures and accelerate the chemical deterioration of concrete or the kinetics of steel corrosion [1]. Cracks located in the structures' concrete cover are particularly detrimental since they represent a direct access to the steel rebars. Nevertheless, the prejudicial impact of cracks on durability can potentially be compensated by their healing capability. An accurate understanding of the impact of cracks and loading on the transfer properties and on the self-healing capacity of concrete is therefore needed to obtain a good prediction of the long-term durability of structures.

Most of the existing studies on the influence of cracking on the transport properties of concrete focused on the effect of cracking on permeability. These investigations were carried out with various kinds of equipment and loading procedures, as summarized in a recent paper [2]. Theoretically, the water flow between two uniform planes increases in function of the cube of their distance according to Poiseuille's law. Practically, unless a crack reaches a threshold width in the concrete matrix, water penetration remains low due to granular interlocking and clogging at crack surfaces. Beyond the threshold crack width, water penetration rises steeply [3–5]. This threshold crack width varies from 0.05 mm to 0.1 mm [2,4–6]. Some studies also showed that presence of fibers in the concrete matrix decreases permeability by limiting crack initiation and propagation [6–8]. The influence of cracking on diffusion is more limited than its effect on permeability because the increase of diffusion is only proportional to the crack opening [9].

The self-healing capability of the concrete matrix has also been examined using permeability tests. It was shown that different physico-chemical phenomena could explain crack self-healing, which results

* Corresponding author.
E-mail address: Jean-Philippe.Charron@polymtl.ca (J.-P. Charron).

0008-8846/$ – see front matter © 2012 Elsevier Ltd. All rights reserved.
doi:10.1016/j.cemconres.2012.03.014

in reduced water permeability over time. The phenomena concern the formation of calcium carbonate $CaCO_3$ [10–14], the continued hydration of the unhydrated cement in concrete [15–17], and the sealing of cracks by water impurities or concrete particles broken during the loading procedures. The kinetics of self-healing is initially fast and then slows significantly [11,13,14,18–21]. Moreover, research works demonstrated that thinner cracks heal faster than larger cracks [11,20,21].

Despite current knowledge about the impact of cracking and self-healing on water transport in concrete, how to take it into account in predictive numerical models of durability and in the design criteria for reinforced concrete structures is not clear. Indeed, there remains a large gap between the laboratory test conditions and in situ conditions, which limits extrapolating current knowledge to structures. Structures are reinforced with steel rebars, support dead loads, and are randomly cracked in service. Nevertheless, most of the trends mentioned above were obtained with permeability tests carried out on single-crack specimens, unreinforced specimens, specimens with unrealistic crack patterns, or unloaded specimens.

A comprehensive research project was launched at the École Polytechnique de Montréal as a first step towards an accurate reproduction of water seepage into structures. The first objective was to develop an innovative device to assess the water permeability of reinforced concrete tie specimens under realistic tensile loadings. The second objective was to demonstrate the gain in durability brought about by including fibers in tie specimens submitted to various loading conditions. The last objective was to determine serviceability design criteria adapted to fiber reinforced concrete. This paper summarizes part of the research related to the second objective. It focuses on determining the water permeability and self-healing capacity of tie specimens with and without fibers submitted to static and constant tensile loadings.

2. Methodology

2.1. Experimental program

Two concrete mixtures were used in this investigation to study the permeability and self-healing of reinforced concrete under loads. The first mixture was a normal strength concrete (NSC) with a water–binder ratio (w/b) of 0.60. The second mixture was a fiber reinforced concrete (FRC) with a w/b of 0.43. Both concretes were selected because they were being studied in ongoing complementary research projects. The impact on the permeability and self-healing results of using materials with different w/b ratio will be explained in the Discussion section. Table 1 provides the mixture compositions of the NSC and FRC. The cement was the same for both concretes; it was a North-American Portland cement type GU (equivalent to European cement CEM1) used for standard application.

The reinforced concrete elements studied in this project were tie specimens. They represent a rebar and the surrounding concrete found in the tensile zone of beams, thick slabs, or walls subjected to bending loads. For these structural elements submitted to bending load, the stress gradient is small and the tensile stress is nearly uniform in the concrete cover. Applying a uniaxial tensile load to the specimen is thus appropriate to represent the state of loading and the resulting cracking pattern of damaged concrete cover in structures. The tie specimens had a length of 610 mm and a prismatic cross-section of 90×90 mm^2 with a centered rebar with a diameter of 11.3 mm. The specimen characteristics were chosen to obtain the concrete cover and crack pattern found in structures [3].

Once the tie specimens were produced, they were demolded after 24 h and stored in lime-saturated water for 3 months before testing. Characterization specimens were produced for each concrete mixture to determine the mechanical properties given in Table 2. The tensile properties of the reinforcing bars were a Young's modulus of 210 GPa, a yield strength of 456 MPa, and an ultimate strength of 563 MPa.

Twenty NSC and thirteen FRC tie specimens were subjected to a static tensile loading until the rebar yielding (Fig. 1a). Ten NSC and seven FRC specimens were instrumented with PI displacement transducers to characterize the crack development under tensile loading. Ten NSC and six FRC specimens served to assess water penetration during loading.

In order to assess the self-healing capability of the concretes under study, another group of tie specimens were submitted to static tensile testing with a period of constant loading (Fig. 1b). The constant loading lasted 6 days and corresponded to an average stress of 250 MPa in the rebar to reproduce a reinforced concrete element with dormant (inactive) cracks under service conditions.

2.2. Measuring devices

The tie specimens were submitted to uniaxial tensile testing with or without simultaneous permeability measurement. The validation for the loading and permeability systems as well as the results analysis procedure can be found in Desmettre and Charron [3]; a summary is provided here.

2.2.1. Tensile loading system

The tie specimens were subjected to uniaxial tensile testing on a 2.5-MN testing machine. Fig. 2a illustrates the instrumentation setup installed on the specimen. The loading was continuously controlled by the average displacement of two linear variable differential transformers (LVDTs) fixed on opposite faces at the ends of the specimen. For static loading, the rate of displacement was set at 0.05 mm/min. For constant loading, the specimen displacement was kept constant. When no permeability measurement was made, the other two opposite faces of the specimen were instrumented with twelve PI displacement transducers to record the crack opening displacement (COD). Once a macrocrack localized in the specimen, the COD was obtained by removing the elastic displacement from the total displacement of the PI transducer. The average stress in the rebar was calculated from the specimen elongation, assuming a perfect bond between the concrete and the rebar.

2.2.2. Permeability system

When the tie specimens were submitted to simultaneous permeability measurement, a sealing membrane was installed on the concrete surface and a permeability cell clamped on (Fig. 2b). The permeability system included a set of two tanks (Fig. 3). The inlet tank was initially filled with water, while the output one remained

Table 1
Composition of the NSC and FRC.

Component	Content (kg/m^3)	
	NSC	FRC
Cement	325	501
Silica fume	0	50
Coarse aggregate (2.5 mm–10 mm)	1002	668
Sand (50 μm–5 mm)	821	801
Superplasticizer (naphthalene sulfonate)	2	8
Water reducing admixture (sodium lignosulfonate)	1	0
Fiber (1%; Dramix 65/35)	0	80
Total water (admixture included)	195	237

Table 2
Mechanical properties of the NSC and FRC measured at 28 days.

Properties	NSC	FRC
Compressive strength (MPa)	37.0	55.0
Tensile strength (MPa)	2.1	2.5
Elasticity modulus (GPa)	31.7	33.0
Poisson's coefficient (−)	0.245	0.260

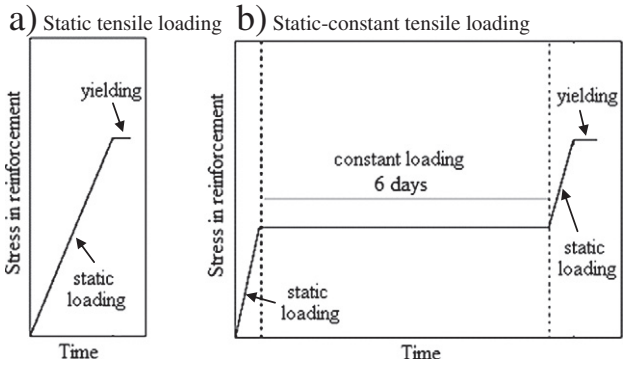

Fig. 1. Loading procedures applied to the tie specimens.a) Static tensile loading, b) static-constant tensile loading.

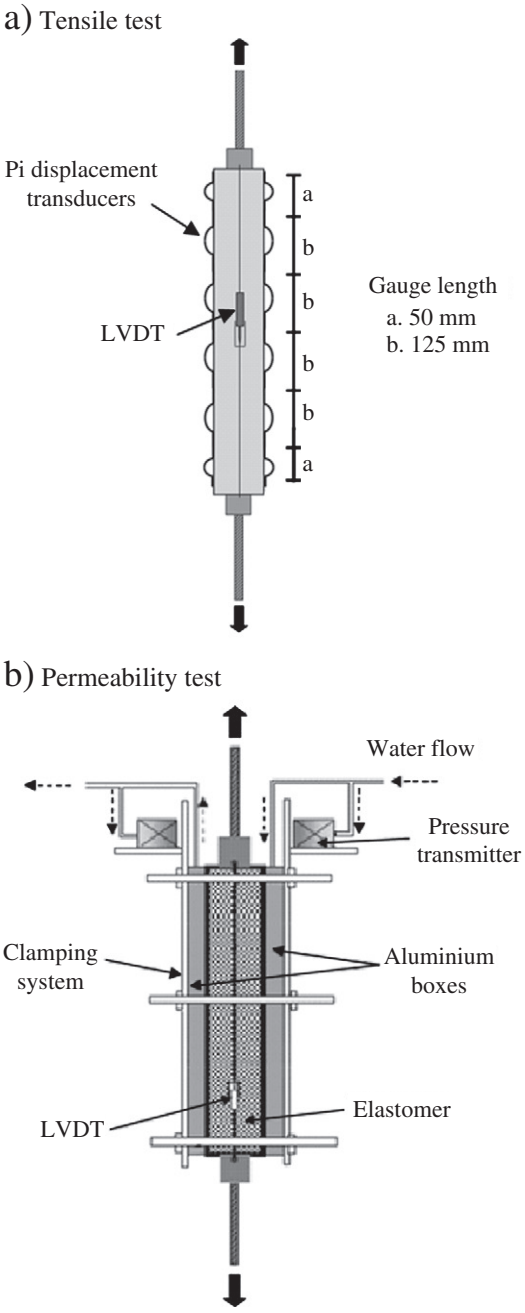

Fig. 2. Instrumentation of the tie specimen.a) Tensile test, b) permeability test.

empty. The tanks were connected to aluminum boxes filled with water and installed upstream and downstream from the tie specimen. All tubing connected to the inlet and outlet tanks were saturated with water. At the beginning of the permeability test, the water in the inlet tank was pressurized to initiate a pressure gradient of 50 kPa to the specimen. As a consequence, water traveled from the inlet tank, through the inlet box, specimen, and outlet box and then to the outlet tank, which remained at the atmospheric pressure. The pressure gradient initiated a unidirectional water flow through the specimen. Two pressure transmitters were installed near the inlet and outlet aluminum boxes (Fig. 2b) to measure the pressure gradient applied to the specimen.

A set of differential pressure transmitters were connected to the base of each tank to continuously measure the amount of water that circulated through the specimen. They recorded changes in tank water height and volume, and provided for computing the associated water flow through the specimen during the permeability test. Fig. 3 depicts one set of tanks for sake of simplicity. Nevertheless, the device included 3 sets of tanks with different diameters to obtain accurate measurement and a sufficient water supply at any time during the test.

The water permeability coefficient K_w (m/s) was calculated with Darcy's law (Eq. (1)), which is often used to describe the water flow through a homogeneous porous medium [9]. In this equation, Q (m^3/s) represents the flow rate, A (m^2) the specimen cross-section, Δh (m) the drop in the hydraulic head across the specimen, and L (m) the specimen thickness. Despite the heterogeneity found in concrete microstructure, a concrete matrix and a uniformly cracked matrix can be considered as homogeneous at a larger scale [22]. It must be mentioned that, in cracked concrete, the water flow is controlled by the crack openings. Between cracks, the water flow is much lower in the concrete matrix and negligible compared to the bulk permeability coefficient determined with Darcy's law.

$$K_w = \frac{Q \cdot L}{A \cdot \Delta h} \tag{1}$$

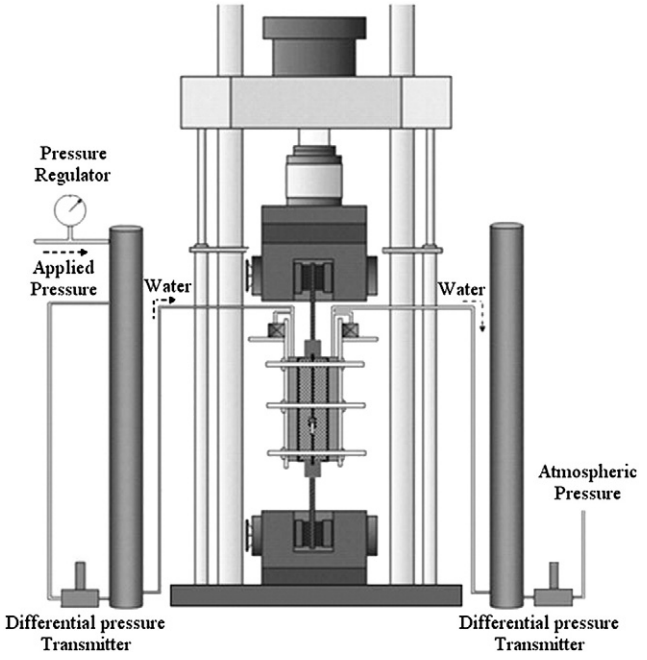

Fig. 3. Water permeability device installed on the universal testing machine.

2.3. Statistical analysis

Statistical analysis was conducted on some experimental results. The variability of results was calculated with Student's Law using Eqs. (2) to (4) [23]. In these equations, X_{mean} is the average value, s the standard deviation, I the interval of confidence, n the number of specimens, and T the student's coefficient. The student's coefficient depends on the number of specimens and the selected percentage of confidence. In this project, the average value X_{mean} was plotted with an interval of confidence of 90%. Table 3 presents the values considered in the statistical analysis of tensile loads and permeability coefficients.

$$I = \left[X_i - T\cdot(s/n)^{1/2}; X_i + T\cdot(s/n)^{1/2}\right] \quad (2)$$

$$s = \frac{\sum_i^n (X_i - X_{mean})^2}{(n-1)} \quad (3)$$

$$X_{mean} = (1/n)\cdot\sum_i^n X_i \quad (4)$$

3. Results

3.1. Mechanical and permeability measurements under static loading

The mechanical behavior of the tie specimens during the static tensile loading was obtained from tensile tests conducted with the instrumentation shown in Fig. 2a. The PI displacement transducers allowed characterization of crack development into the specimens. Fig. 4a presents the typical load–displacement curves for the NSC and FRC specimens. Different phases can be distinguished. At the beginning, the curve presents a linear phase, associated with the material's elastic behavior. Microcracks then appear, and the curve becomes nonlinear. Microcracks propagate and merge to form a localized macrocrack. Other macrocracks occur and develop until reaching the rebar yielding. As the macrocracks formed, the tie specimen's rigidity decreased, resulting in a decrease in curve slope. Sudden drops of force occurred when the macrocracks localized and propagated through the cross section of the tie specimen due to a release of energy in the test setup. These drops were less pronounced for the FRC specimens than for their NSC counterparts. The contribution of the concrete to the total tensile strength of the tie specimens was higher with the FRC than with the NSC, resulting in greater forces before reaching the rebar yielding.

When a macrocrack appeared, the PI displacement transducers measured the COD. Fig. 4b shows COD evolution during the tests depicted in Fig. 4a. More cracks and thinner cracks developed in the FRC specimen in comparison to the NSC specimen. For example, at rebar yielding, the three cracks in the NSC specimen had CODs greater than the maximum COD of around 0.25 mm measured in the four cracks in the FRC specimen. The formation of new macrocracks frequently resulted in an instantaneous reduction of the CODs of the existing macrocracks.

Table 3
Parameters for the determination of an interval of confidence of 90%.

Parameters	Tensile load F (kN)		Permeability K_w (m/s)	
	Fig. 5		Fig. 7b	
	NSC	FRC	NSC	FRC
Statistical value	F[a]	F[a]	K_w[b]	K_w[b]
Percent of confidence (%)	90	90	90	90
Number of specimens (−)	10	7	10	6/4[c]
Student's coefficient (−) [23]	1.833	1.943	1.833	2.015/2.353[c]

[a] F: Tensile force.
[b] K_w: Permeability coefficient;
[c] At $\sigma_s \geq 350$ MPa, n is equal to 4 and T changes to 2.353.

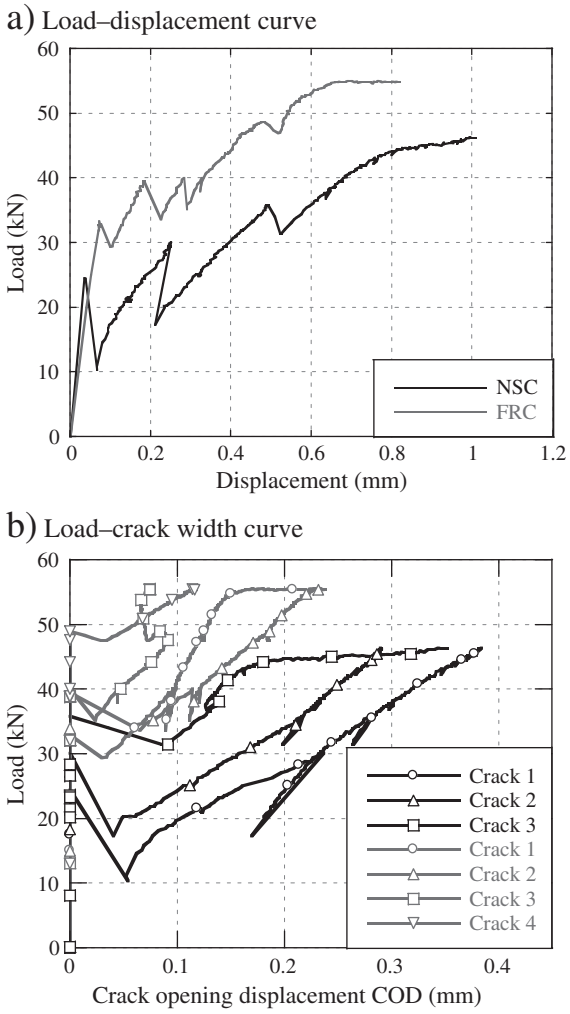

Fig. 4. Typical tensile behavior of the NSC and FRC tie specimens under static loading.a) Load–displacement curve, b) load–crack width curve.

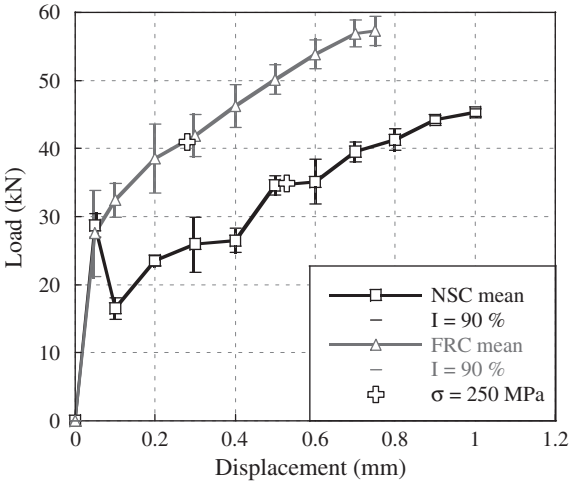

Fig. 5. Variability of the tensile behavior of the NSC and FRC tie specimens under static loading.

Fig. 5 shows the plots of the mean value of the load-displacement curves and the interval of confidence of 90% for the NSC and FRC tie specimens, based on the statistical parameters detailed in Table 3. The intervals of confidence calculated are small and thus illustrates the good reproducibility observed in the mechanical behavior of the NSC and FRC tie specimens. The FRC presented a better load-carrying capacity and rigidity than the NSC. In the cracked state and for the same displacement, the force applied to the NSC specimens was equal to 60%–70% of that applied to the FRC specimens.

Fig. 6 shows a typical curve representing changes in the water permeability coefficient versus the average stress in the rebar for an NSC tie specimen during the loading procedure detailed in Fig. 1a. Changes in the permeability coefficient during loading are closely related to the material's mechanical behavior, and thus can be divided into different regimes. Firstly, the permeability coefficient can be considered constant during the elastic phase of the tensile loading (2×10^{-10} m/s). Then, microcracks appear and propagate, resulting in a very slight increase in the permeability (from 2×10^{-10} m/s to 4×10^{-10} m/s). A sudden increase in permeability (from 4×10^{-10} m/s to 1×10^{-6} m/s) occurs when the first macrocrack localizes. Finally, other macrocracks form and develop, and permeability increases until the rebar yielding. At this stage, the permeability is close to 1×10^{-5} m/s. Such permeability results can be plotted on a logarithmic scale to focus on low permeability values (Fig. 6a) or a linear scale to bring out the increased permeability of the cracked concrete (Fig. 6b). The second option was selected for the following results.

Fig. 7a summarizes the permeability results for all the NSC and FRC tie specimens subjected to tensile static loading. At a same stress level in reinforcement, there is a dispersion in the permeability values, related to the inherent variability of the materials. Nevertheless, the results obtained for each material were collected in two quite distinct zones. For the same stress levels in the rebar, the FRC tie specimens were less permeable than the NSC specimens. Fig. 7b represents the mean value with the interval of confidence of 90%, calculated with the parameters listed in Table 3. There were only 4 data for the FRC tie specimens with a stress level superior to 350 MPa, resulting in a larger interval of confidence at the highest stress levels. When the tie specimen was cracked, the average permeability was 60%–70% lower with the FRC than with the NSC.

3.2. Mechanical and permeability measurements under constant loading

The loading procedure was modified to measure the permeability change with time and estimate the self-healing capacity of the materials. The variation consisted in maintaining the loading constant over 6 days at an average stress level in the rebar of 250 MPa (Fig. 1b). This stress level was chosen as being representative of admissible loading applied to reinforced concrete under service conditions. The crosses in Fig. 5 indicate the force at which stress in the rebar reached 250 MPa (34.8 kN and 41.0 kN for the NSC and FRC specimens respectively).

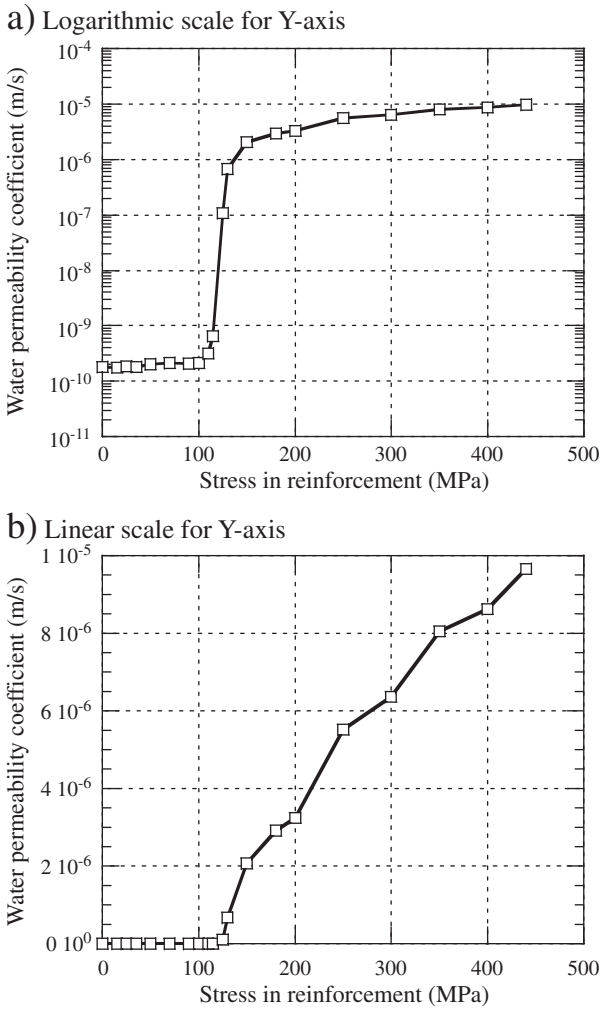

Fig. 6. Water permeability coefficient versus the stress in reinforcement in the NSC.a) Logarithmic scale for Y-axis, (b) linear scale for Y-axis.

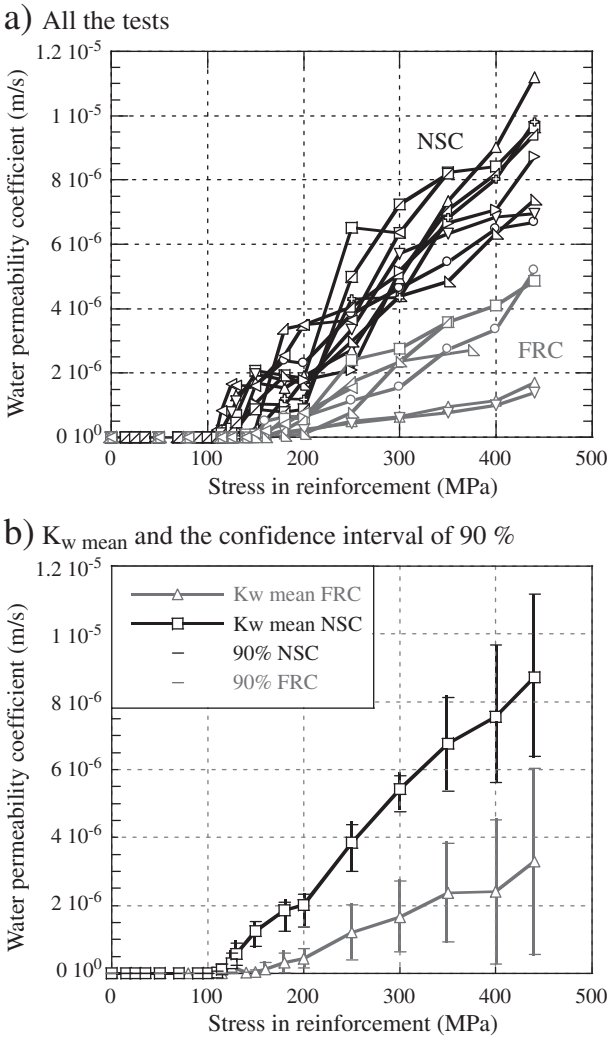

Fig. 7. Permeability under static loading for the NSC and FRC.a) all the tests, b) $K_{w\ mean}$ and the confidence interval of 90%.

Fig. 8 plots the changes in crack opening during the constant loading. It confirms that the COD measured on the tie specimen remained nearly constant during such a loading. A negligible increase in COD (less than 0.018 mm) was observed in the first 24 to 48 h before stabilization. It represents around 6% of the initial COD values. Complementary tests demonstrated that these results were the upper limits.

Fig. 9a shows the evolution of permeability coefficients during the 6 days of constant loading. All curves indicate similar self-healing kinetics. The permeability coefficient decreased rapidly at the beginning of the constant phase, with the reduction rate slowing down after 24 h. The evolution of the relative permeability coefficient (K_w/K_{wi}) is plotted in Fig. 9b, based on the average results obtained for each material. The initial permeability coefficient K_{wi} corresponds to the effective permeability coefficient at the beginning of the constant phase, before self-healing occurred. Firstly, the value of K_{wi}, for a stress level of 250 MPa in the rebar, was lower for the FRC (1.4×10^{-6} m/s) than for the NSC specimens (3.4×10^{-6} m/s). Secondly, the decrease in the relative permeability coefficient with time was also more pronounced with the FRC than with the NSC, particularly in the first 24 h.

Once the constant phase of 6 days was completed, the loading of the tie specimens continued (reloading phase) until the rebar yielded (Fig. 1b). Fig. 10 shows the evolution of the water permeability coefficient during the first static loading, the constant phase, and the static reloading. During the reloading phase, the water permeability coefficient increased. The stress enhancement $\Delta\sigma$ needed to reach the initial permeability coefficient K_{wi} (value of K_w at the beginning of the constant phase before self-healing occurred) is summarized in Table 4 for different conditions. In addition to the specimens tested with constant loading around 250 MPa, other tests were performed with a constant loading at 150 MPa with the NSC specimens and around 350 MPa with the FRC specimens. Table 4 indicates that a $\Delta\sigma$ of 20–35 MPa was needed to reach the initial permeability coefficient K_{wi} for the NSC tie specimens, whereas 40–60 MPa was required for the FRC tie specimens.

4. Discussion

4.1. Mechanical and permeability measurements under static loading

The results presented in Figs. 4 and 7 show that the intensity of water penetration during the static tensile loading was closely linked to the mechanical behavior of the tie specimens. The elastic phase and the formation of microcracks in the specimen had negligible influence on its permeability, whereas localization and development of macrocracks significantly increased permeability. These results are in good accordance with the research works of Gérard [24] and Lawler et al. [6].

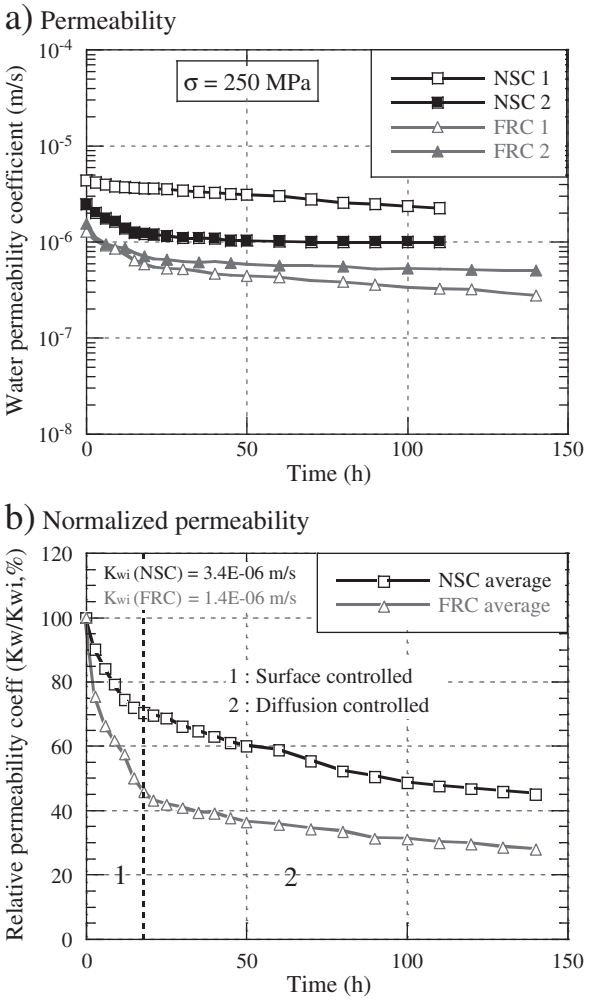

Fig. 9. Permeability under constant loading for the NSC and FRC.a) Permeability, b) Normalized permeability.

The mechanical behavior and permeability measurement were clearly modified by the utilization of FRC instead of NSC in the tie specimens (Figs. 4, 5, and 7). Two parameters may be considered responsible for these modifications, the differences in the w/b ratio and the fiber content of the materials.

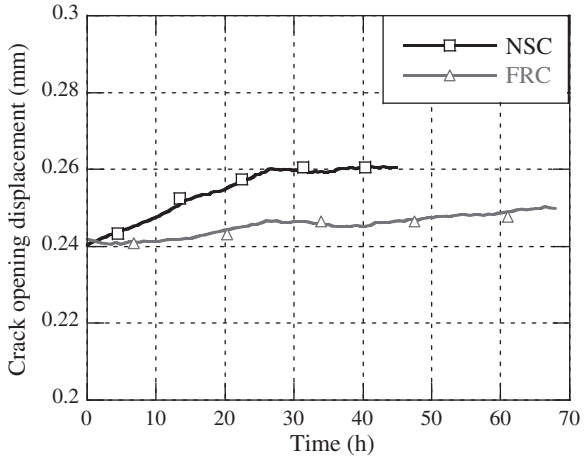

Fig. 8. Crack opening evolution under constant loading.

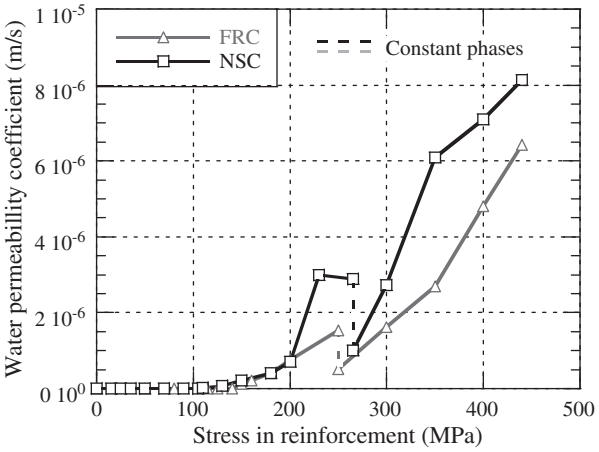

Fig. 10. Impact of reloading on permeability.

Table 4
Reloading needed to reach the initial coefficient K_{wi}.

Parameter	NSC1	NSC2	FRC1	FRC2	FRC3
σ_s of the constant phase (MPa)	150	265	250	350	375
$K_{wi\ (initial)}$ (m/s)	9.39^{E-07}	2.89^{E-06}	1.54^{E-06}	3.59^{E-06}	2.71^{E-06}
$K_{wf\ (final)}$ (m/s)	2.42^{E-07}	1.00^{E-06}	5.05^{E-07}	1.61^{E-06}	9.65^{E-07}
$\Delta\sigma_{Kw=Kwi}$ (MPa)	20	35	50	40	60

In a mechanical point of view, the difference in the w/b ratio should not have influenced significantly the tie specimens strength and stiffness after cracking, because the tensile post-peak behavior is similar between 37 MPa and 55 MPa concretes without fibers. However, addition of fibers to a concrete mixture is known to delay crack initiation and propagation, and to provide higher stiffness and tensile capacity once cracks appear [25]. Fig. 4 shows that more and thinner cracks formed in the FRC tie specimens. Logically, the stiffness, load recovery after cracking, and load-carrying capacity of those specimens were notably improved in their cracked state compared to the NSC tie specimens. Fig. 5 illustrates that the impact on the mechanical behavior of the fibers inclusion is statistically significant in spite of the inherent variation in properties of NSC and FRC. Consequently, a greater force had to be applied to the FRC specimens in comparison to the NSC specimens to reach an identical level of stress in the rebar.

In a permeability point of view, the difference in the w/b ratio (or in the binder content) of the materials should not have modified significantly the water permeability of the tie specimens either. Indeed, in cracked state, the flow rate through the whole specimen is largely controlled by cracks and much less by the concrete matrix. Consequently, as soon as the tie specimens crack, the permeability results under static loading are essentially influenced by the cracking pattern and the crack openings in the tie specimens. The fiber content of the FRC, which led to the formation of thinner, rougher and numerous cracks as well as crack branching in the tie specimens, limited water seepage. The mechanical behavior and the cracking pattern provided by the fiber reinforcement is thus responsible for the lower permeability observed at cracked state in the FRC than in the NSC specimens at any stress level in the rebar (Fig. 7). The permeability coefficient in the cracked state was approximately 60–70% lower in the FRC at any stress level. This trend is statistically significant even when considering the variability in results (Fig. 7b).

Considering that the FRC tie specimens supported higher loads and presented lower water permeability for equivalent stresses in the rebar, adding fibers to the concrete mixture clearly favors the long-term durability.

4.2. Mechanical and permeability measurements under constant loading

The permeability measurement on the cracked NSC and FRC tie specimens submitted to a constant loading allowed the estimation of the water flow reduction with time and the assessment of the self-healing phenomenon (Fig. 9). The kinetics of the water flow reduction can be divided into two phases. The decreasing rate was initially fast, then became slower and tended to stabilize. This trend is in good accordance with the observations of Edvardsen [14], Clear [11], and Reinhardt and Jooss [20]. The decreasing rate cannot be related to crack width variation, since Fig. 8 shows that the CODs remained constant during the constant loading. Thus, the concrete's self-healing capacity was responsible for the reduced permeability.

In order to identify the phenomenon causing the self-healing, the healed specimens were sawn on both sides of the cracks, perpendicular to the axis of loading, at the end of the permeability test. The sawn samples were kept in desiccators containing drierite and lime to prevent carbonation before analysis. The two sides of the cracks were separated just before scanning electron microscopy (SEM) observation. Fig. 11a shows one of the pictures taken of the healed crack surfaces. Fig. 11b is the corresponding X-ray spectra for the products marked by a cross in Fig. 11a. The analysis confirmed a uniform formation of calcium-carbonate ($CaCO_3$) crystals at the crack surfaces during the self-healing process, thus reducing the effective crack width for the water flow. This result was also supported by the presence of white precipitates on the specimens at crack locations. Continued hydration of unhydrated cement may have occurred at the same time, but C–S–H products were not observed on the crack surfaces.

The identification of $CaCO_3$ as the main phenomenon responsible for the self-healing in the 3-month-old concrete mixtures is in good agreement with observations found in the literature for mature specimens that contain small amounts of unhydrated cement. Therefore, the two phases of the self-healing kinetics illustrated in Fig. 9b can be explained by $CaCO_3$ growth [14]. In a first phase, the crystals growth was surfaced controlled as long as Ca^{2+} ions were directly available on the crack surfaces. Then, a diffusion process through the concrete matrix was necessary to provide supplementary Ca^{2+} ions at the surface and initiate the formation of $CaCO_3$. This second phase occurred slower, so the rate of self-healing decreased.

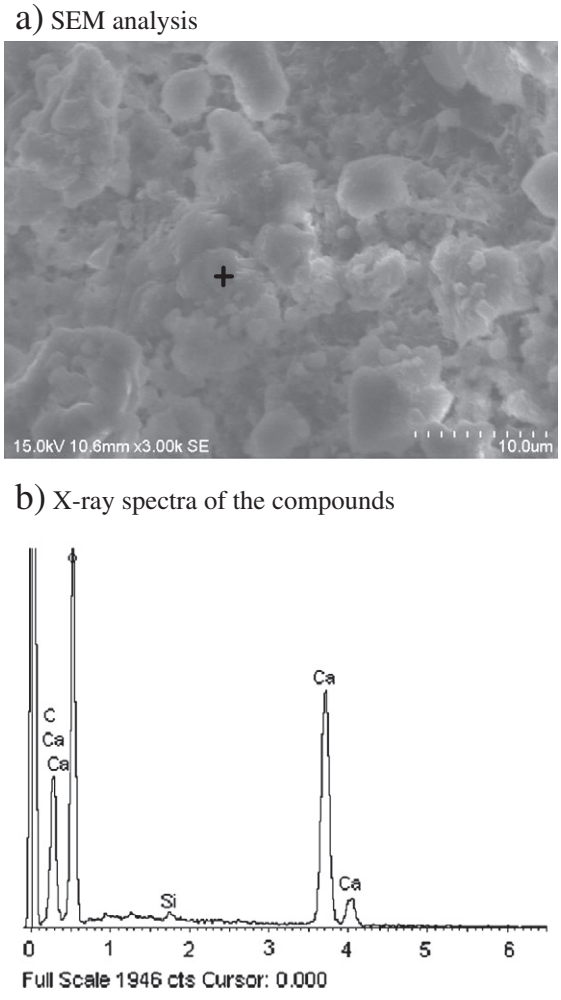

Fig. 11. Characterization of products formed in cracks.a) SEM analysis, b) X-ray spectra of the compounds.

Besides, Fig. 9b showed that the self-healing phenomenon was faster in the FRC than in the NSC tie specimens, particularly during the first phase of $CaCO_3$ formation. This observation is not related to the difference in the w/b ratio (or in the binder content) of the materials. Indeed, the experimental program was carried out on mature concretes containing limited amount of unhydrated cement available for reaction at crack surfaces and the formation of $CaCO_3$ therefore controlled the self-healing. Some researchers observed the same phenomenon and demonstrated the negligible impact of the w/b ratio on the self-healing for mature cracked concrete [13,21]. Moreover, complementary permeability tests were carried out in this project to evaluate the effect of the w/b ratio on self-healing. NSC and FRC tie specimens with a similar initial permeability coefficient presented identical rate and amplitude of self-healing under constant loading [26]. Consequently, the higher self-healing capacity of the FRC tie specimens is associated to their specific cracking pattern.

After the self-healing process occurred during the constant loading, the static loading was continued for some tie specimens up to the rebar yielding (Fig. 1b). The results presented in Table 4 and Fig. 10 indicate that the permeability reduction resulting from the self-healing of dormant cracks was not instantaneously lost during this reloading. A loading of 20–35 MPa and 40–60 MPa had to be applied to the NSC and FRC specimens respectively, at the end of the constant phase, to achieve the initial permeability coefficient K_{wi} measured before the self-healing had begun. This reloading amplitude is related to the energy required to reopen cracks to their initial widths. Again, this result highlighted the potential contribution of FRC in decreasing water penetration in reinforced concrete structures.

5. Conclusion

The research project aimed to assess the water permeability and self-healing of NSC and FRC tie specimens subjected to static and constant tensile loadings. The following conclusions can be drawn.

- Adding fibers to a concrete mixture delayed crack initiation and propagation, thereby providing more cracks, thinner cracks, and crack branching. This led to higher rigidity, load recovery after cracking, and load-carrying capacity of the FRC tie specimens in comparison to the NSC ones.
- The crack pattern of the FRC tie specimens led to permeability coefficients approximately 60–70% lower in the cracked state than that of the NSC tie specimens at any stress level in the rebar. This trend was statistically significant even when considering the variability of results.
- After 6 days of constant loading at an average stress level of 250 MPa in the rebar, self-healing had reduced water penetration by 50% and 70% in the NSC and FRC specimens, respectively. The self-healing capacity seems to be maximized initially with thinner cracks such as those found in FRC.
- The main phenomenon responsible for self-healing in the 3-month-old concrete mixtures was the formation of $CaCO_3$ crystals. This observation may be different for mixtures with high unhydrated-cement contents such as ultra-high performance concrete.
- For the studied experimental conditions, the kinetics of self-healing with $CaCO_3$ crystals was rapid and surfaced-controlled for approximately 24 h. Then, a slower diffusion process took place continuing $CaCO_3$ formation.
- The additional loading required after a constant loading phase to reopen cracks to their effective widths before self-healing occurred was about 20–60 MPa in the rebar. These values may change according to the healing period and the concrete involved.
- The low water permeability and high self-healing capacity of the FRC mixture confirmed its potential to improve the long-term durability of reinforced concrete structures.

Acknowledgement

The research project was financially supported by the Québec Research Fund on Nature and Technology (FQRNT). The authors are grateful to Professor Gagné's research team (University of Sherbooke) for their participation in the SEM observations.

References

[1] B. Gérard, S. Jacobsen, J. Marchand, Concrete cracks II: observation and permeability — a review, Concrete under severe conditions, Environment and Loading, 2, 1998, pp. 183–197.
[2] M. Hoseini, V. Bindiganavile, N. Banthia, The effect of mechanical stress on permeability of concrete: a review, Cem. Concr. Compos. 31 (2009) 213–220.
[3] C. Desmettre, J.-P. Charron, Novel water permeability device for reinforced concrete, Mater. Struct. 44 (2011) 1713–1723.
[4] C.M. Aldea, M. Ghandehari, S.P. Shah, A. Karr, Estimation of water flow through cracked concrete under load, ACI Mater. J. 97 (2000) 567–575.
[5] K. Wang, D.C. Jansen, S.P. Shah, A.F. Karr, Permeability study of cracked concrete, Cem. Concr. Res. 27 (1997) 381–393.
[6] J.S. Lawler, D. Zampini, S.P. Shah, Permeability of cracked hybrid fiber-reinforced mortar under load, ACI Mater. J. 99 (2002) 379–385.
[7] J. Rapoport, C.M. Aldea, S.P. Shah, M. Asce, B. Ankenman, A. Karr, Permeability of cracked steel fiber-reinforced concrete, J. Mater. Civ. Eng. 14 (2002) 355–358.
[8] M. Tsukamoto, J.-D. Wörner, Permeability of cracked fibre-reinforced concrete, Ann. J. Concr. Concr. Struct. 6 (1991) 123–135.
[9] B. Gérard, H.W. Reinhardt, D. Breysse, Measured transport in cracked concrete, in: H.W. Reinhardt (Ed.), RILEM Report 16 — Penetration and Permeability of Concrete : Barriers to Organic and Contaminating Liquids, E & FN Spon, Stuttgart, Germany, 1997, pp. 265–324.
[10] M.W. Loving, Autogenous healing of concrete, Bulletin, No.13, American Concrete Pipe Asoociation, 1936.
[11] C.A. Clear, The effects of autogenous healing upon the leakage of water through cracks in concrete, Technical Report 559, Cement and Concrete Association, Wexham Springs, 1985.
[12] D. Homma, H. Mihashi, T. Nishiwaki, Self-healing capability of fibre reinforced cementitious composites, J. Adv. Concr. Technol. 7 (2009) 217–228.
[13] K.R. Lauer, F.O. Slate, Autogenous healing of cement paste, J. Am. Concr. Inst. 27 (1956) 1083–1097.
[14] C. Edvardsen, Water permeability and autogenous healing of cracks in concrete, ACI Mater. J. 96 (1999) 448–454.
[15] M. Li, V.C. Li, Cracking and healing of engineered cementitious composites under chloride environment, ACI Mater. J. 108 (2011) 333–340.
[16] E. Schlangen, N.T. Ter Heide, K. Van Breugel, Crack healing of early age cracks in concrete, in: M.S. Konsta-Gdoutos (Ed.), Measuring, Monitoring and Modeling Concrete Properties, 2006, pp. 273–284.
[17] W. Zhong, W. Yao, Influence of damage degree on self-healing of concrete, Constr. Build. Mater. 22 (2008) 1137–1142.
[18] A. Hosoda, S. Komatsu, T. Ahn, T. Kishi, S. Ikeno, K. Kobayashi, Self healing properties with various crack widths under continuous water leakage, in: A.e. al (Ed.), Concrete Repair, Rehabilitation and Retrofitting II, Taylor & Francis Group, London, 2009, pp. 221–227.
[19] W. Ramm, M. Biscoping, Autogenous healing and reinforcement corrosion in water penetrated separation cracks, 13th International Conference on Structural Mechanics in Reactor Technology (SMiRT 13), Porto Alegre, Brazil, August 13–18 1995.
[20] H.W. Reinhardt, M. Jooss, Permeability and self-healing of cracked concrete as a function of temperature and crack width, Cem. Concr. Res. 33 (2003) 981–985.
[21] M. Argouges, R. Gagné, Étude des mécanismes et de la cinétique de l'autocicatrisation dans des morties cimentaires fissurés, Dixième édition des Journées scientifiques du Regroupement francophone pour la recherche et la formation sur le béton $(RF)^2B$, Cachan, France, 2009.
[22] D. Breysse, B. Gérard, Transport of fluids in cracked media, in: H.W. Reinhardt (Ed.), Rilem Report 16 — Penetration and Permeability of Concrete : Barriers Toorganic and Contaminating Liquids, E & FN Spon, Stuttgart, Germany, 1997, pp. 123–154.
[23] S. Alalouf, D. Labelle, J. Ménard, Introduction à la Statistique Appliquée, Deuxième édition Éditions Addison-Wesley, 1990.
[24] B. Gérard, Contribution des couplages mécaniques-chimie-transfert dans la tenue à long terme des ouvrages de stockage de déchets radioactifs, Ecole normale supérieure de Cachan, Cachan, FRANCE, 1996.
[25] P. Rossi, Les bétons de fibres métalliques, Presses de l'École Nationale des Ponts et Chaussées, 1998.
[26] C. Desmettre, Contribution à l'étude de la perméabilité du béton armé sous sollicitations statiques et cycliques, École Polytechnique de Montréal, Montréal, QC, Canada, 2012.